Size effects in the far-infrared magneto-optical absorption of small bismuth particles

R. E. Sherriff* and R. P. Devaty
Department of Physics and Astronomy, University of Pittsburgh, Pittsburgh, Pennsylvania 15260
(Received 20 July 1992; revised manuscript received 22 March 1993)

Small bismuth particles are studied as a model system for a three-dimensionally confined solid-state plasma. Information on the carrier dynamics is obtained from far-infrared magneto-optical absorption measurements. Samples consisted of pellets pressed from a mixture of bismuth particles, prepared by inert gas evaporation, and an insulating host with the volume fraction of bismuth less than 0.01. The spectra were taken from 10 to 350 cm^{-1} by Fourier-transform spectroscopy with the samples typically immersed in liquid helium. Particles with diameters around 0.5 μm show an abundance of magnetic-field-dependent resonances that can be successfully described by a semiclassical treatment for the solid-state plasma using bulk bismuth parameters. As the mean particle diameter is reduced to 150 Å, the data show a dramatic change from a rich spectrum of field-dependent resonances to strong field-independent absorption. This is markedly different behavior than that observed for semiconductor quantum dots, for which field-dependent absorption is seen even in the smallest structures. Despite relatively broad size distributions within the bismuth powders, a size-specific sum-rule analysis associates the field-dependent absorption with particles larger than approximately 200 nm in diameter.

I. INTRODUCTION

Small metal particles have been investigated for many years due to the interesting electronic and optical properties they exhibit.[1,2] These properties result from the confinement of carriers within the particles. Recent advances in nanofabrication techniques now permit the construction of similar systems in semiconductors for which carriers are confined in three dimensions typically by the lateral confinement of a two dimensional (2D) electron gas. The size of the confined plasmas in these structures can range from micrometers, for which the carriers behave classically,[3] to a few hundred Angstroms for which confinement leads to quantum-mechanical effects.[4–10]

Because of the low carrier density ($\sim 3\times 10^{17}$ cm^{-3}) and small effective masses in the semimetal bismuth, small bismuth particles are analogous in many ways to semiconductor particles and quantum dots. In particular, the carrier cyclotron energies can be made equal to or greater than other relevant energies (the plasmon energy, the Fermi energy, etc.) allowing interesting magnetoplasma behavior to be observed in the laboratory. Unlike semiconductor systems, however, the solid-state plasma confined in a small bismuth particle is a multicomponent plasma containing both electrons and holes, and the effective masses for all of the carriers are extremely anisotropic. The result is a qualitative difference in magneto-optical behavior and increased complexity relative to a single-component plasma. Figure 1(a) shows the fan diagram for the electric dipole resonances of a small particle containing a single-component isotropic Drude plasma. Plasma-shifted cyclotron resonance is observed. At low fields, the modes are plasmonlike in character (the small-particle sphere resonance), while at high fields the mode with the correct circular polarization asymptotically approaches the frequency of bulk cyclotron resonance. Simple models for semiconductor quantum dots lead to similar diagrams. Figure 1(b) shows the fan diagram for a two-component plasma for which the two charge carriers have the same sign and density, but different effective masses. In addition to a plasmon-shifted cyclotron resonance, there is an additional resonance for which the frequency vanishes in the absence of an external magnetic field. At low fields, this resonance is a hybrid cyclotron resonance involving the motion of both carriers. At high magnetic fields, the resonance frequency asymptotically approaches the cyclotron frequency of the carrier with the higher effective mass. In this paper we classify resonances according to their semiclassical behavior at low fields. If the resonance frequency vanishes at zero field, the resonance is called a low-frequency hybrid resonance. If the resonance frequency is nonzero at zero field, the resonance is called a high-frequency resonance or plasma resonance.

The presence of the hybrid resonances is an important distinction between small Bi particles and semiconductor particles. As the size of a Bi particle is decreased, quantum confinement will lead to discrete energy levels with a minimum energy-level spacing at the Fermi energy. For sufficiently small particles, the frequency associated with transitions between discrete levels lies in the far infrared, and there will be a *qualitative* change in the behavior of the low-frequency hybrid resonances, i.e., the zero-field resonance frequencies must be nonzero.

In this paper, far-infrared (FIR) magneto-optical absorption spectroscopy is used to study the behavior of carriers confined in small bismuth particles supported in an insulating medium. Earlier work showed that the rich magneto-optical spectrum of unsupported bismuth particles with sizes on the order of 1 μm could be described successfully using a simple semiclassical model.[11] As the particle size is decreased from microns to hundreds of Angstroms, the FIR absorption spectrum changes dramatically from a large number of magnetic-field-

dependent resonances to strong field-independent absorption. This behavior is quite different from that observed for the single-component plasmas in quantum dots, which exhibit field-dependent behavior even at very small sizes.[4–10]

The presentation begins with a brief discussion of the semiclassical calculation used to model the FIR absorption of micron-sized bismuth particles in Sec. II. Section III provides details of the experimental apparatus, information on the samples, and a description of the techniques used in extracting absorption information from the FIR spectra. Experimental results are given in Sec. IV. Section V discusses the results and presents a size-specific sum-rule analysis that can be used to set a rough lower limit of 200 nm on the diameter of particles responsible for the observed field-dependent absorption.

II. SEMICLASSICAL MODEL FOR BISMUTH PARTICLES

The semiclassical model[11] consists of a Drude calculation of the effective dielectric tensor of the four-component carrier plasma in bismuth followed by a quasistatic calculation of the absorption coefficient associated with a sphere with this dielectric function. The model yields the expression

$$\alpha_{\mathrm{ED}}(\omega)=\frac{9\sqrt{\epsilon_0}f\omega}{2c}\mathrm{Im}(\hat{\mathbf{E}}^{(e)*}\cdot\mathbf{T}^{-1}\cdot\hat{\mathbf{E}}^{(e)}) , \tag{1}$$

for the electric dipole absorption coefficient where

$$\mathbf{T}=\mathbf{I}+2\epsilon_0\boldsymbol{\epsilon}(\omega)^{-1} . \tag{2}$$

Here $\mathbf{I}$ is the identity matrix, f is the volume fraction of bismuth in the sample, $\hat{\mathbf{E}}^{(e)}$ is the polarization unit vector of the electric field of the incident wave, ϵ_0 is the frequency-independent dielectric constant of the substrate, and $\boldsymbol{\epsilon}(\omega)$ is the dielectric tensor of the bismuth particle. The magnetic dipole absorption coefficient is given by

$$\alpha_{\mathrm{MD}}(\omega)=\frac{2\pi}{5}\sqrt{\epsilon_0}fa^2\frac{\omega^2}{c^3}\mathrm{Re}(\hat{\mathbf{B}}^*\cdot\bar{\boldsymbol{\sigma}}\cdot\hat{\mathbf{B}}) , \tag{3}$$

where a is the particle radius, $\hat{\mathbf{B}}$ indicates the direction of the magnetic field of the incident radiation, and $\bar{\boldsymbol{\sigma}}$ is the effective conductivity tensor, which can be expressed in terms of the resistivity tensor $\boldsymbol{\rho}$ by $\bar{\boldsymbol{\sigma}}\equiv\bar{\boldsymbol{\rho}}^{-1}$ with

$$\bar{\boldsymbol{\rho}}\equiv\tfrac{1}{2}[\mathrm{Tr}(\boldsymbol{\rho})\mathbf{I}-\boldsymbol{\rho}^{\dagger}] , \tag{4}$$

where the symbol Tr( ) specifies the trace operation and the dagger indicates the transpose operation. Magnetic dipole absorption can only be considered separately from electric quadrupole absorption as is done here due to the large static dielectric tensor of bismuth.[12]

Notice that both Eqs. (1) and (3) depend explicitly on the orientation of the bismuth particle with respect to the static magnetic field. This dependence implies that an average over particle orientation must be performed to calculate the absorption coefficient expected from the random distribution of orientations within a real sample. Because of the complexity of the expressions, this average is evaluated numerically[13] to yield theoretical spectra at specific magnetic fields. Figure 2 shows a typical theoretical spectrum for the magnetic dipole absorption coefficient of 2000-Å-diameter particles at 3.0 T calculated using $1/(2\pi c\tau)=1$ cm^{-1} and an ensemble of 400 randomly chosen orientations. As this spectrum demonstrates, the distribution of orientations produces broad regions of absorption with inhomogeneous line shapes. Some strong resonance peaks can be identified within these regions as arrows in the figure indicate, but many weaker resonances and shoulders are more difficult to label unambiguously.

The magnetic-field dependence of the strong resonance peaks can be presented in a fan diagram as shown in Fig. 3. Some information contained in the complicated shapes of the absorption regions is of necessity lost in such a representation, but the fan diagram is still a useful tool for visualizing the general field dependence of the absorption. Varying resonance strengths, widths, and line shapes as well as noise resulting from the small ensemble size used in the numerical average make it difficult to unambiguously track all of the resonances throughout the frequen-

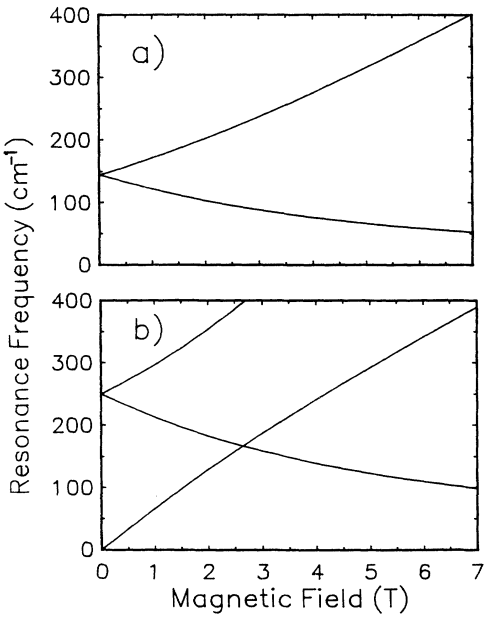

FIG. 1. Illustration of the qualitative difference in the predicted magneto-optical behavior of a two-component semiclassical plasma relative to a single-component plasma. (a) Calculated fan diagram showing plasma-shifted cyclotron resonance for a single-component Drude plasma with cyclotron frequency/magnetic field $\omega_{c1}/H=50$ cm^{-1}/T and plasma frequency $\omega_{p1}=250$ cm^{-1}, corresponding to a carrier density $n_1=1.30\times10^{16}$ cm^{-3} and an effective mass $m_1^*/m_0=1.87\times10^{-2}$. (b) Calculated fan diagram for a two-component Drude plasma made by adding a second carrier with $\omega_{c2}/H=100$ cm^{-1}/T, $\omega_{p2}=353$ cm^{-1}, corresponding to $n_2=1.3\times10^{16}$ cm^{-3} and $m_2^*/m_0=9.34\times10^{-3}$, to the plasma in (a). The appearance of the hybrid cyclotronlike resonance for which the frequency approaches zero with vanishing magnetic field is a qualitative difference in behavior. The magneto-optical behavior of a semiclassical small bismuth particle is far more complex, as shown in Figs. 3–5 in Ref. 13.

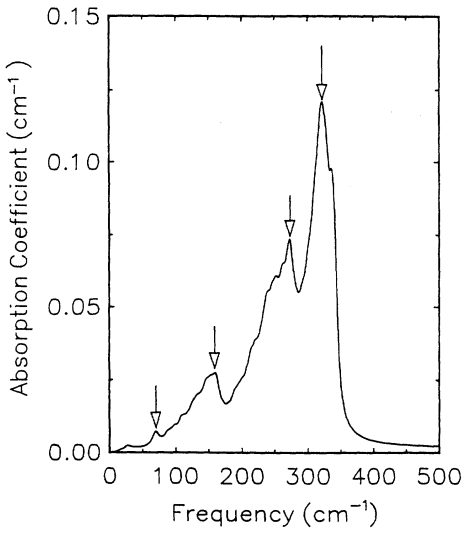

FIG. 2. Calculated magnetic dipole absorption coefficient for 2000-Å-diameter Bi particles in a 3-T magnetic field. The effects of averaging over 400 randomly chosen particle orientations are included. Arrows indicate separable regions of strong absorption.

cy range. Gaps in the theoretical curves shown in Fig. 3 and their general coarse nature are a result of these tracking complications.

Despite these minor difficulties, the model clearly predicts a number of electric and magnetic dipole resonances. As in the two-component Drude plasma, two distinct types of resonances are observed at low magnetic fields. Modes that approach a nonzero frequency at zero field involve the collective dipole oscillation of the plasma. These are generalizations of the plasma-shifted cyclotron resonance observed in both the single- and two-component plasmas. Modes that go to zero frequency at zero field are generalizations of the hybrid cyclotronlike resonance seen for the two-component plasma. These hybrid modes do not occur in a single-component 3D confined plasma. With increasing magnetic field, the modes mix and at very high fields the high-frequency modes approach bulk cyclotron frequencies.

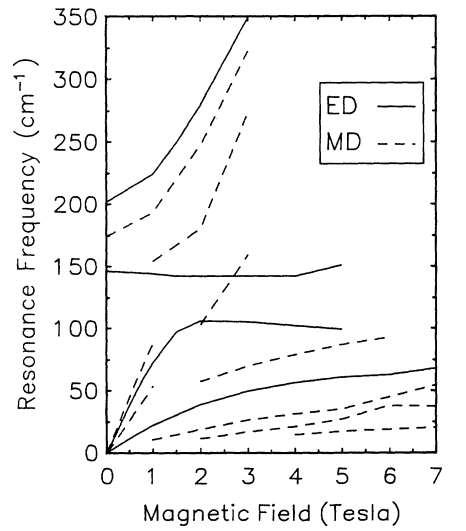

FIG. 3. Resonance frequency vs magnetic field for both electric dipole (ED) and magnetic dipole (MD) absorption obtained from the semiclassical model, including orientational averaging. Coarseness of the curves results from both the small number of magnetic fields and the small ensemble of particle orientations used in the numerical averaging process.

III. EXPERIMENT

Bismuth particles were made by inert gas evaporation.[14] This process yields a bismuth "smoke" typically with a log normal distribution of particle sizes. The mean particle diameter is controlled by the molecular weight and pressure of the inert gas. Estimates of the mean particle diameter and the size distribution were made by transmission electron microscope examination of copper supported carbon film microscopy grids that were inside the collection jar during the evaporation. Selected area electron diffraction patterns suggest that small bismuth particles are crystalline with the same lattice constants as bulk bismuth.

Table I lists the Bi powders used in this experiment along with evaporation conditions and size information. Both $\bar{d}$, the arithmetic mean diameter, and $\bar{d}_v$, the root-mean-cube diameter, are given. The latter is essentially the volume weighted mean and is therefore more indicative of the particle sizes dominating the FIR absorption. Powder 1 has the largest $\bar{d}_v$ due to the long tail of large particles in its size distribution, as shown in Fig. 4. Powders 3, 4, and 5 all have similar mean values significantly smaller than the size estimates for powder 1, but Fig. 5 demonstrates that they have noticeably different distributions. It will be seen that these differences result in noticeably different FIR absorption behavior as well. Powder 6 has by far the smallest values for both $\bar{d}$ and $\bar{d}_v$, which fall close to the peak of the sharp size distribution shown in Fig. 6. Clearly, the complete size distribution must be considered to obtain any information on the size dependence of the absorption.

The samples used for this study were made by the classic "KBr" pellet method. The Bi powder obtained from inert gas evaporation is mixed with an insulating host and the mixture is crushed in a hydraulic press at a force of 8–9 tons. The resulting pellet is about 0.5 in. in diameter

TABLE I. Summary of Bi powders used in the experiment. Both the mean ($\bar{d}$) and root-mean-cube ($\bar{d}_v$) diameter for each powder are listed.

Bi powder No.	Evaporation conditions	$\bar{d}$ (nm)	$\bar{d}_v$ (nm)
1	40 torr Ar	76	165
2	10 torr Ar	78	106
3	50 torr He		
4	20 torr He	72	104
5	10 torr He	88	112
6	2.5 torr He	14.5	15.5

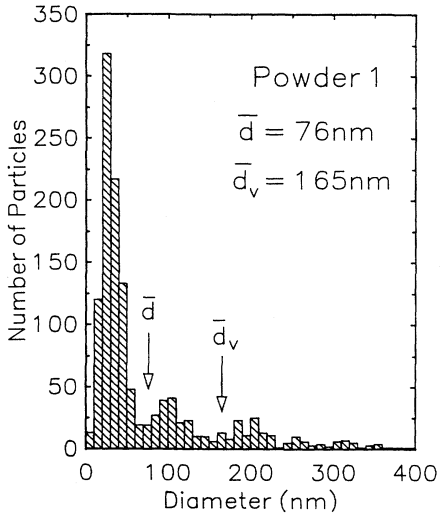

FIG. 4. Size distribution for Bi powder 1. The mean diameter $\bar{d}$ and the root-mean-cube diameter $\bar{d}_v$ are indicated. Powder 1 contains the largest Bi particles.

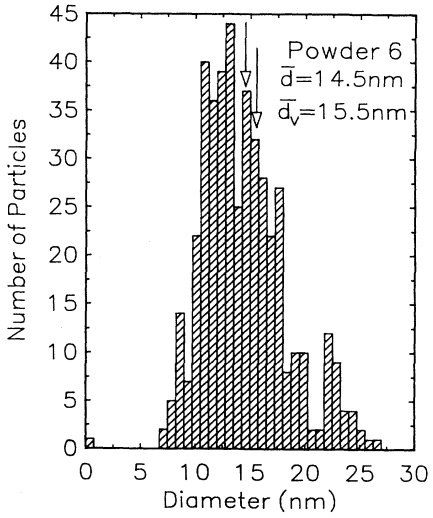

FIG. 6. Size distribution for Bi powder 6. This is the sharpest size distribution among the powders and has the smallest values for both $\bar{d}$ and $\bar{d}_v$.

and 2- to 4-mm thick. To reduce clustering of the Bi particles within the samples, pellets are ground to a fine powder and repressed five times. Samples are generally made with the volume fraction of bismuth at or below 0.01 with the actual amount chosen according to the strength of the absorption in the desired frequency region.

This variation in the amount of bismuth is necessary due to the disparity in strength of different resonances. The low-frequency hybrid resonances tend to be rather weak. To see such modes requires relatively bismuth-rich samples with $f=0.01$. The stronger plasma mode (at zero field) resonances that occur at higher frequencies imply the need for f of 0.0025 to 0.001 or the transmission of the absorption peak will be insufficient for accurate absorption measurements. This difference in strength implies the need for two sets of samples: those optimized for low frequencies ($\omega < 100$ cm^{-1}) and those intended for high frequencies ($\omega > 100$ cm^{-1}). At low magnetic fields, the low-frequency resonances are cyclotronlike in character, whereas the high-frequency resonances are plasmonlike.

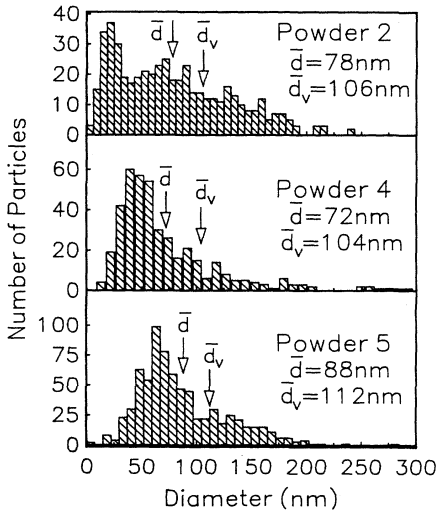

FIG. 5. Size distribution for Bi powders 2, 4, and 5 along with indications of $\bar{d}$ and $\bar{d}_v$. Note that while the mean values are similar for these three powders the distributions are noticeably different.

Low FIR absorption in the appropriate frequency region motivates the selection of the supporting host insulator for pressed pellets in both frequency regions. The host material must also be compatible with the randomization procedure. A teflonlike polymer[15] called DLX-6000 is used for samples intended for low-frequency studies. DLX-6000 transmits at low frequencies but shows a rapidly increasing absorption[16] above 100 cm^{-1}. Cesium iodide (CsI) is used as the substrate for pellets optimized for high-frequency studies, since its reststrahl absorption extends from 65 to 130 cm^{-1}. The region above 130 cm^{-1} is absorption-free making it acceptable for use in pellets designed to study the plasmon modes.

FIR transmission spectra for the samples were obtained by Fourier-transform spectroscopy from 10 to 350 cm^{-1} using a Michelson interferometer and a 1.5-K Si composite bolometer. For measurements at zero magnetic field, samples were immersed in liquid helium at 4.2 K in a commercial liquid helium bucket dewar. Magneto-optical spectroscopy was conducted with samples in the bore of a liquid-helium-cooled superconducting solenoid. Samples in the magnet cryostat were typically immersed in liquid helium with temperatures at or below 4.2 K.

The FIR power absorption coefficient $\alpha(\omega)$ can be extracted from transmission measurements by using data from two samples with identical composition but different thicknesses. $\alpha(\omega)$ is given by

$$\alpha(\omega)=\frac{1}{x_1-x_2}\ln\frac{T_2(\omega)}{T_1(\omega)}\ , \tag{5}$$

where T_i and x_i refer to the transmission and thickness of the sample indicated by the subscript.[17] This expression is an approximation valid when the reflectivity of the samples is the same and when multiple reflections are not important. The large absorption of even low volume fraction bismuth pellets makes the approximation a reasonable one for the bismuth composite samples.

Due to the difference in character of the resonances in the two frequency regions, a slightly different treatment for the data is required in each case. The low-frequency hybrid resonances do not absorb at $\mathbf{H}=\mathbf{0}$. Thus, it is possible to trace the frequency of field-dependent resonances by only looking at the field-induced change in the absorption coefficient $\Delta\alpha(\omega,\mathbf{H})$, which is given by

$$\Delta\alpha(\omega,\mathbf{H})\equiv\alpha(\omega,\mathbf{H})-\alpha(\omega,\mathbf{0})=-\frac{1}{x}\ln\frac{T(\omega,\mathbf{H})}{T(\omega,\mathbf{0})}\ . \tag{6}$$

where $T(\omega,\mathbf{H})$ is the sample transmission at magnetic field $\mathbf{H}$ and x is the sample thickness. Notice that the measurement is made on a single sample and the loss due to reflection is approximately the same for the sample at both $\mathbf{H}\neq\mathbf{0}$ and $\mathbf{H}=\mathbf{0}$. Changes in transmission are therefore due solely to changing absorption.

Plasma modes that exist in the high-frequency region *do* have absorption at $\mathbf{H}=\mathbf{0}$. In fact, the sphere resonance peak absorption is strongest at zero field. This property makes it difficult to interpret the shift of resonance peaks by using only $\Delta\alpha(\omega,\mathbf{H})$. For this reason, two measurements are taken for the high-frequency samples. $\Delta\alpha(\omega,\mathbf{H})$ is measured for a single pellet in the magnet cryostat just as for the low-frequency pellets. Then a second experiment is performed on two similar samples in a zero-field cryostat to find $\alpha(\omega,\mathbf{H}=\mathbf{0})$ from Eq. (5). The total absorption coefficient at a given field $\alpha(\omega,\mathbf{H})$ can be found by combining the two measurements to obtain

$$\alpha(\omega,\mathbf{H})=\alpha(\omega,\mathbf{0})+\Delta\alpha(\omega,\mathbf{H})\ . \tag{7}$$

Peak positions are then read directly off of the $\alpha(\omega,\mathbf{H})$ spectra. The only drawback to this technique is that field-independent absorption (substrate absorption and/or Bi absorption not due to free carriers) is not suppressed as it is when only $\Delta\alpha(\omega,\mathbf{H})$ is plotted. Such background absorption is subtracted off all the high-frequency pellet spectra to clarify the field-dependent behavior. The method used to approximate this background will be detailed when the results are presented.

One additional minor complication in the case of the pellets designed for study of the high-frequency plasma modes is the slight variation in f used to optimize the level of absorption. Fortunately, for noninteracting particles the absorption coefficient depends linearly on the volume fraction. The effect of different volume fractions can therefore be removed by simply normalizing the $\alpha(\omega,\mathbf{H})$ spectra by f.

IV. RESULTS

The bismuth powders can be separated into three groups according to their FIR absorption behavior. Powders 1 and 2 show field-dependent absorption behavior described by the semiclassical model. Powders 3, 4, and 5 show weaker absorption with dramatically simpler field dependence. Powder 6 shows little or no field-dependent absorption but does show increased field-independent absorption over the other samples. Table II summarizes the volume fraction normalized field-dependent and field-independent absorption for all of the powders. Data presented in the remainder of this section include spectra for typical samples in both the high- and low-frequency regions along with fan diagrams of resonance frequency versus magnetic field for all of the samples.

All of the high-frequency absorption spectra are normalized by the bismuth volume fraction to aid in comparison. Also keep in mind that the high-frequency curves for a sample are constructed from a set of $\Delta\alpha(\omega,\mathbf{H})$ curves taken at different fields and a single $\alpha(\omega,\mathbf{0})$ measurement. Any fine structure that appears at the same frequency in all of the $\alpha(\omega,\mathbf{H})/f$ curves is therefore almost certainly noise in the $\alpha(\omega,\mathbf{0})$ spectrum.

Figure 7 shows the volume fraction normalized absorption spectra for Bi (powder 1) in the high-frequency region. The zero-field spectrum shows a distinct resonance at about 155 cm^{-1} which is clearly magnetic-field dependent. A large field-independent background, however, makes interpretation of the resonance behavior difficult. To highlight the field dependence of the resonances, a fit to the field-independent background is subtracted from the data. The fit is obtained by estimating the minimum absorption coefficient observed at each individual frequency as the magnetic field is increased from 0 to 8.5 T. The dot-dashed line in Fig. 7 indicates the background fit used for powder 1. A similar process is applied to the high-frequency data for all the powders. The resulting field-dependent absorption spectra for powder 1 are plotted in Fig. 8 with a small dc offset separating the curves for clarity. Several broad resonances can be identified as the zero-field resonance splits. Positions for the resonances at fields between 1 and 3 T are obtained by fitting the data with three Lorentzians.

TABLE II. Summary of volume fraction normalized field-dependent and field-independent absorption observed for bismuth powders. ω_{Pk} is the zero-field resonance frequency, $\alpha_{FD}(\omega_{Pk})/f$ is the peak strength of the field-dependent resonance at zero field, and α_{FI}/f is the strength of the field-independent absorption at 250 cm^{-1}.

Bi powder No.	ω_{Pk} (cm^{-1})	$\alpha_{FD}(\omega_{Pk})/f$ (cm^{-1})	α_{FI}/f (cm^{-1})
1	155	1700	4300
2	188	780	3800
3	219	445	4000
4	210	490	3250
5	212	340	3300
6			5900

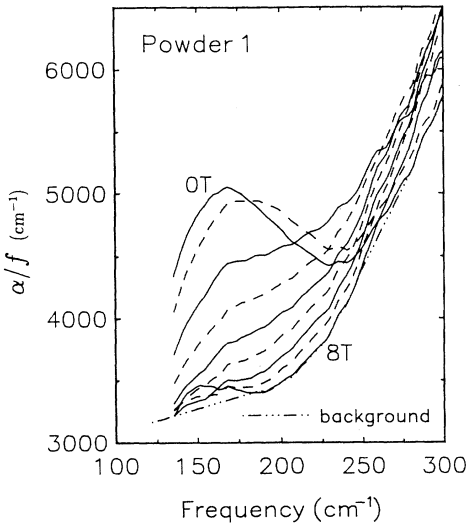

FIG. 7. Absorption of Bi powder 1 in the high-frequency region. The absorption coefficient has been normalized by the volume fraction $f=0.0027$. Spectra are plotted for integer fields from 0 to 8 T. The curves are in order of increasing magnetic field along the line joining the 0- and 8-T labels with solid lines for even integer fields and dashed lines for odd integer fields. The dot-dashed line is an estimate of the field-independent background.

The change in absorption coefficient with magnetic field for powder 1 at low frequencies is shown in Fig. 9 as a three-dimensional plot of absorption spectra versus magnetic field. Two modes with strong field dependence can be seen moving quickly through the frequency region at fields below 2 T. A third very distinct mode appears

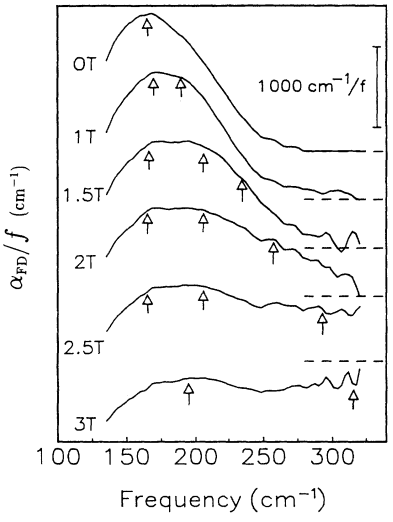

FIG. 8. Field-dependent absorption for Bi powder 1 obtained by subtraction of the field-independent background from the α/f spectra shown in Fig. 6. The curves have been offset vertically for clarity. Each dashed line on the right gives the zero level for the spectrum immediately above it. Resonance frequencies are indicated by arrows. Resonance frequencies for fields between 1.5 and 2.5 T were obtained by fitting the spectra with three Lorentzians.

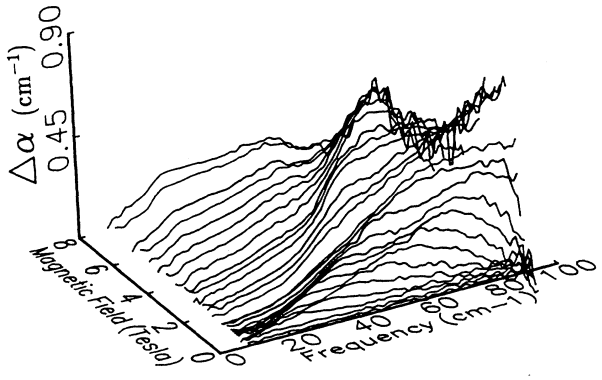

FIG. 9. The change in the absorption coefficient of Bi powder 1 with magnetic field in the low-frequency region. [Note: $\Delta\alpha(\omega)$ is not normalized by the bismuth volume fraction.]

above 60 cm^{-1} for fields above 3 T. A broad plateau of absorption appears at lower frequencies and high fields.

Like the calculated absorption spectra discussed in Sec. II, the experimental spectra show broad regions of absorption which contain some strong resonance peaks and many weaker shoulders. The field dependence of the strong peaks observed for powder 1 is plotted along with the predictions of the semiclassical model in Fig. 10. The bars placed on selected points in the figure provide estimates of the regions of strong absorption that surround these peaks rather than errors in peak location. The field dependence of the resonance peaks shows the qualitative behavior predicted by the semiclassical model. In particular, note that plasma modes and low-frequency hybrid

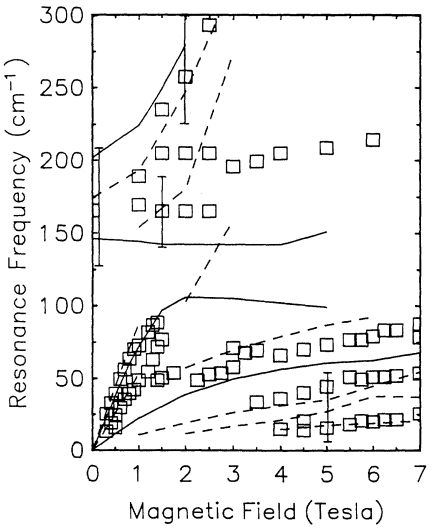

FIG. 10. Fan diagram for Bi powder 1. Predictions of the semiclassical model are also plotted with solid lines indicating electric dipole modes and dashed lines indicating magnetic dipole modes. Bars on selected points are estimates of the width of the inhomogeneous resonance regions rather than errors in the resonance peak frequencies.

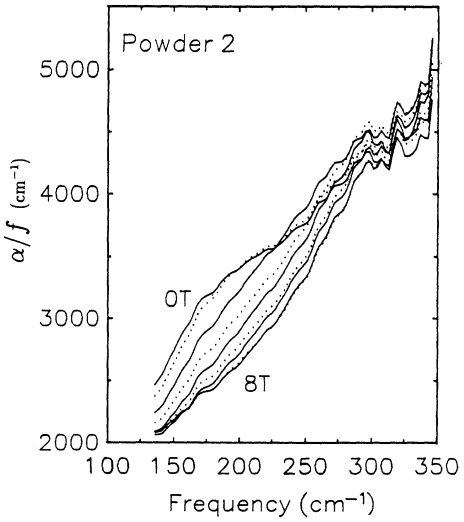

FIG. 11. Absorption of Bi powder 2 in the high-frequency region. The absorption coefficient has been normalized by the volume fraction $f=0.0025$. Spectra are plotted for integer fields from 0 to 8 T. The curves are in order of increasing magnetic field along the line joining the 0- and 8-T labels with solid lines for even integral fields and dotted lines for odd integer fields.

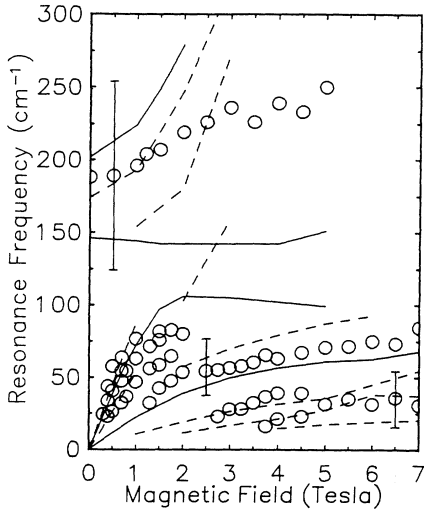

FIG. 13. Fan diagram for Bi powder 2. Predictions of the semiclassical model are also plotted with solid lines indicating electric dipole modes and dashed lines indicating magnetic dipole modes. Bars on selected points are estimates of the width of the inhomogeneous resonance regions rather than errors in the resonance peak frequencies.

cyclotron modes of both electric dipole and magnetic dipole absorption can be identified in the data. The data also show the splitting of the sphere resonance as the model predicts although the frequency of the lower branch is higher than expected.

High-frequency data for powder 2 are presented in Fig. 11. For this sample, the zero-field resonance is smaller and broader than that observed for powder 1, but the field-independent background is about the same. Again, the minimum observed absorption (in this case the 8-T spectrum) was subtracted from the spectra. The background corrected spectra show a peak that shifts upward slightly with increasing field and broadens inhomogeneously toward higher frequencies. Distinct splitting as seen in larger particles is not apparent. Note that the

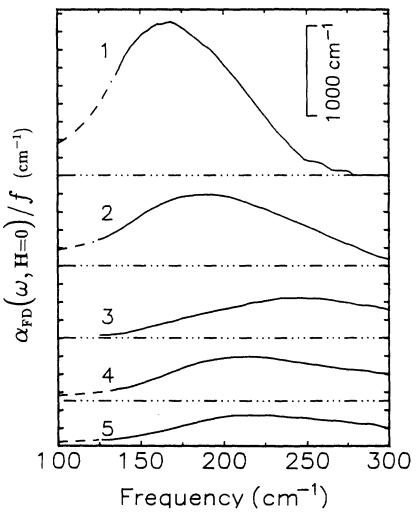

FIG. 12. Comparison of the zero-field sphere resonance for Bi powders 1–5. All curves have had a field-independent background subtracted. Dot-dashed lines indicate the zero level for each curve. The dashed lines are the Lorentzian fits used to extrapolate the data into the CsI reststrahl region for the sum-rule analysis.

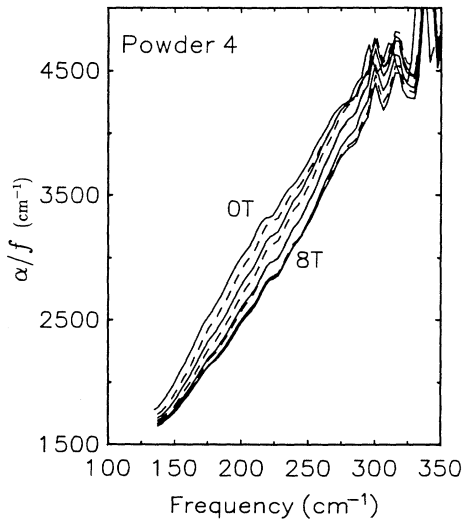

FIG. 14. Absorption of Bi powder 4 in the high-frequency region showing behavior typical of the intermediate sized powders 3, 4, and 5. The absorption coefficient has been normalized by the volume fraction $f=0.0025$. Spectra were plotted for integer fields from 0 to 8 T. The curves are in order of increasing magnetic field along the line joining the 0- and 8-T labels with solid lines for even integer fields and dashed lines for odd integer fields.

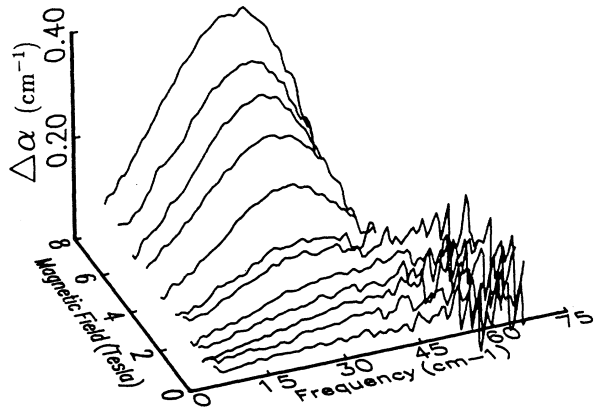

FIG. 15. The change in the absorption coefficient with magnetic field for Bi powder 4 in the low-frequency region showing behavior typical of the intermediate sized powders 3, 4, and 5.

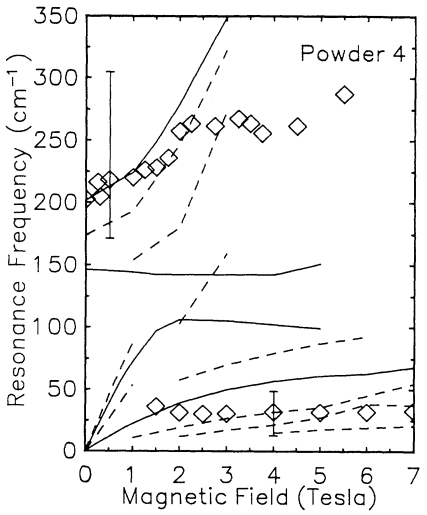

FIG. 17. Fan diagram for Bi powder 4. Predictions of the semiclassical model are also plotted with solid lines indicating electric dipole modes and dashed lines indicating magnetic dipole modes. Bars on selected points are estimates of the widths of the inhomogeneous resonance regions rather than errors in the resonance peak frequencies.

zero-field peak position and resonance strength are substantially different from powder 1, as the comparison in Fig. 12 demonstrates. The peak is now at 188 cm^{-1} and the strength is reduced to 780 cm^{-1}. The low-frequency absorption region for powder 2 is similar to that seen for powder 1 in that several field-dependent resonances are apparent. However, weaker and broader absorption along with an anomalous decrease in absorption $[\Delta\alpha(\omega,\mathbf{H})<0]$ for fields above 4 T complicate tracking of resonance frequencies. This decrease in absorption would result if there is an unexpected zero-field resonance at about 70 cm^{-1} that shifts with increasing field. However, it is more probable that it is due to shifting of the zero-field sphere resonance near 200 cm^{-1} to higher frequencies. Identification of resonance frequencies in the low-frequency region is made assuming that this second explanation is indeed correct. The powder 2 fan diagram in Fig. 13 still shows a reasonable agreement with the behavior predicted by the model, but the scatter in resonance frequencies is larger than obtained for powder 1 and the high-frequency resonance splitting is no longer observed.

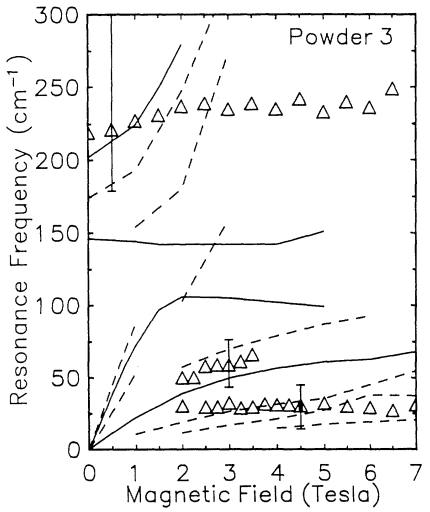

FIG. 16. Fan diagram for Bi powder 3. Predictions of the semiclassical model are also plotted with solid lines indicating electric dipole modes and dashed lines indicating magnetic dipole modes. Bars on selected points are estimates of the widths of the inhomogeneous resonance regions rather than errors in the resonance peak frequencies.

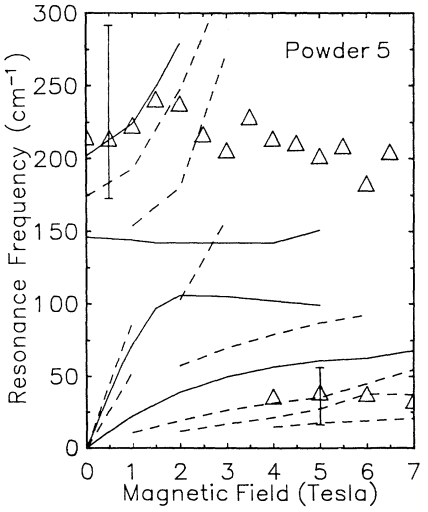

FIG. 18. Fan diagram for Bi powder 5. Predictions of the semiclassical model are also plotted with solid lines indicating electric dipole modes and dashed lines indicating magnetic dipole modes. Bars on selected points are estimates of the widths of the inhomogeneous resonance regions rather than errors in the resonance peak frequencies.

Spectra for powders 3, 4, and 5 are typified in both frequency regions by the data for powder 4 shown in Figs. 14 and 15. The field-dependent absorption in the high-frequency region is even weaker than that observed in powder 2. The background corrected zero-field spectra for all three intermediate-sized powders are compared to the curves for powders 1 and 2 in Fig. 12. Zero-field absorption for the intermediate powders is peaked at higher frequencies and is weaker in strength than the absorption of the larger particles.

The change in absorption for intermediate-sized powders in the low-frequency region is even more dramatic. Instead of an abundance of modes there is much less complicated behavior. The fan diagrams in Figs. 16–18 highlight the change. The powder 3 fan diagram has two modes at low frequency and one at high frequency, while the fan diagrams for powders 4 and 5 show only one mode in each frequency region. Notice that the resonance frequencies in these powders show a very weak dependence on magnetic field. Even more striking is the complete absence of the low-frequency hybrid cyclotronlike modes that tend to zero frequency at zero field.

For the particles in powder 6, only the slightest of field-dependent effects was seen against a substantial amount of noise. In both frequency regions there is a small change in the overall level of absorption with magnetic field but no resonance features can be observed. The high noise level present is due to a significant increase in the field-independent background, which is now 5900 at 250 cm^{-1}. Attempts to improve the quality of the data by reducing the amount of bismuth in the sample (and therefore the level of the field-independent absorption) are actually counterproductive since the field-dependent absorption is also reduced.

V. DISCUSSION

Four principal effects can be identified in the size dependence of the magneto-optical spectra as the bismuth particle size distribution shifts toward smaller particles. (i) The low-frequency hybrid modes, which tend to zero frequency as the magnetic field is reduced, vanish. (ii) The zero-field plasma resonance peak frequency shifts upwards. (iii) The strength of the field-dependent absorption in both frequency regions decreases. (iv) The field-independent bismuth absorption increases.

Disappearance of the low-frequency hybrid modes with decreasing size is perhaps the most pronounced change in the spectra. This may be related to the onset of quantum confinement of the free carriers. The low carrier density and small effective masses for Bi lead to large deBroglie wavelengths and therefore to quantum effects for relatively large particles. An exact calculation of quantization energies for carriers in a small Bi particle is complicated by the extreme anisotropy of the carrier effective masses. However, we can obtain a rough estimate of the energy levels by considering a single carrier with an isotropic effective mass in a spherical square well with an infinite barrier. Using the lightest bulk Bi cyclotron mass, we get an energy-level separation of about 150 cm^{-1} for a 1000-Å-diameter particle. Quantum size effects will make an important contribution to the energies of observed transitions if the energy-level spacing is comparable to or exceeds the plasma energies ($\sim\hbar\omega_P$) and/or the cyclotron energies ($\sim\hbar\omega_c$). In addition, confinement effects should play a role in the observed spectra if $a \lesssim v_F/\omega_c$ where a is the particle radius and v_F the Fermi velocity. For a 3D electron gas this condition becomes $a \lesssim (\hbar c/eB)(3\pi^2 n)^{1/3}$. For sufficiently small particles, incoherent boundary scattering may broaden the lines so that they are not observed even if the semiclassical model is valid. If $n = 3\times 10^{17}$ cm^{-3}, as appropriate for Bi, boundary effects may play a role for $B \lesssim 2.7$ T for a 1000-Å-diameter particle.

Notice that the fan diagram for powder 3 shown in Fig. 16 has a pair of modes at low frequency that extrapolate to about 30 cm^{-1} at zero field but no low-frequency hybrid modes. This behavior is similar to some results seen in semiconductor structures[4–10] that confine a single carrier type. In those single-component systems the FIR behavior is typically independent of the number of carriers confined. This is explained by a generalization of Kohn's theorem.[18] It has not yet been shown that the theorem can be further generalized to a system with several types of carriers all having different anisotropic masses as are found in Bi. It is also not clear that the bare confining potential for carriers in small Bi particles is parabolic.

Unlike the absorption seen in semiconductor structures or quantum dots, however, the smallest Bi particles show little or no field-dependent absorption. This startling contrast may be the result of the quantum confinement energy pushing the valence and conduction bands apart and thereby removing the small band overlap that is the origin of the free carriers in bismuth. Even without quantum-mechanical effects, however, there may be no free carriers left in the smallest Bi particles. Inversion of the bulk Bi carrier density suggests that each electron-hole pair occupies a volume roughly equivalent to a 200-Å-diameter sphere. The mean particle diameter in powder 6 is $\sim$150 Å.

While the disappearance of the low-frequency hybrid modes and the shift in the zero-field plasma resonance frequency are qualitative indications of the onset of quantum confinement, the changing strengths observed for both the field-dependent and field-independent absorption may be used to obtain rough quantitative information about the size dependence. The field-dependent resonance frequencies agree with the semiclassical model for large particles and the strength of these resonances decreases in samples for which the size distribution is shifted to smaller diameters. At the same time, the field-independent absorption increases with increasing numbers of smaller particles. This behavior suggests that the field-dependent resonances are due mainly to absorption by particles above a certain radius a_c and that the field-independent background is associated with some or all of the particles smaller than a_c. If this is so, then it is possible to develop a sum rule for individual particle sizes and use it to estimate a_c.

The analysis begins with the sum rule for a composite medium,[19]

$$\int_0^\infty n(\omega)\alpha(\omega)d\omega=\pi f\omega_p^2/2c \ , \tag{8}$$

in which $\alpha(\omega)$ is the absorption coefficient, $n(\omega)$ is the real part of the index of refraction for the composite medium, and ω_p is the bulk plasma frequency of the metal. If the particles are treated as independent absorbers, then the total absorption can be written as an integral over the size distribution,

$$\alpha(\omega)=\int_0^\infty \alpha(a,\omega)da \ , \tag{9}$$

where $\alpha(a,\omega)$ is an absorption density and a is the particle radius. Furthermore, the volume fraction f of metal can be written in a similar way as an integral over the volume fraction density,

$$f=\int_0^\infty f(a)da \ . \tag{10}$$

Substitution of these integrals into the sum rule and a change in the order of integration yields

$$\int_0^\infty da\left[\int_0^\infty n(\omega)\alpha(a,\omega)d\omega-\frac{\pi}{2c}f(a)\omega_p^2\right]=0 \ , \tag{11}$$

which leads to a new size specific sum rule,

$$\int_0^\infty n(\omega)\alpha(a,\omega)d\omega=\pi f(a)\omega_p^2/2c \ . \tag{12}$$

This is basically the composite sum rule in Eq. (8) applied to each particle radius. This result is not surprising since the assumption that the particles are independent implies that a sample with a size distribution is equivalent to a "stack" of samples each containing only one particle size but with volume fractions appropriately chosen.

The experimental absorption spectra can be divided into field-dependent resonances and a field-independent background,

$$\alpha(\omega,\mathbf{H})=\alpha_{\mathrm{FD}}(\omega,\mathbf{H})+\alpha_{\mathrm{FI}}(\omega) \ . \tag{13}$$

Under the assumption that the field-dependent resonances are the result of absorption in particles with radii above a_c, the two parts of the absorption coefficient can be written as

$$\begin{aligned}\alpha_{\mathrm{FD}}&=\int_{a_c}^\infty \alpha(a)da \ ,\\ \alpha_{\mathrm{FI}}&=\int_0^{a_c}\alpha(a)da \ .\end{aligned} \tag{14}$$

By integrating the particle sum rule [Eq. (12)] over the appropriate range of particle sizes one obtains

$$\int_0^\infty n(\omega)\alpha_{\mathrm{FD}}(\omega)d\omega=\frac{\pi\omega_p^2}{2c}\int_{a_c}^\infty f(a)da \ . \tag{15}$$

This sum rule associates the strength α_{FD} with the volume fraction of particles above the critical radius a_c.

To evaluate the right side of Eq. (15) the size-specific volume fraction $f(a)$ can be expressed in terms of the particle size distribution $\eta(a)$ by

$$f(a)=\frac{1}{V}\eta(a)\frac{4\pi a^3}{3} \ , \tag{16}$$

where V is the volume of the sample. If it is assumed that the particle size histograms obtained by electron microscopy are representative of all the particles in the sample, then the actual particle distribution $\eta(a)$ for the entire sample can be written as a multiple of the measured histogram $\eta'(a)$ so that $\eta(a)=\gamma\eta'(a)$. The normalization constant γ can be found from the requirement that

$$f=\frac{\gamma}{V}\int_0^\infty \eta'(a)\frac{4\pi a^3}{3}da \ . \tag{17}$$

After solving for γ, $\eta(a)$ can be written as

$$\eta(a)=\eta'(a)\frac{3fV}{4\pi}\left[\int_0^\infty \eta'(a)a^3da\right]^{-1} \ . \tag{18}$$

Substitution for $f(a)$ in terms of $\eta(a)$ in Eq. (15) then produces

$$\int_0^\infty n(\omega)\alpha_{\mathrm{FD}}(\omega)d\omega=\frac{\pi\omega_p^2 f}{2c}\left[\int_0^\infty \eta'(a)a^3da\right]^{-1}\times\int_{a_c}^\infty \eta'(a)a^3da \ . \tag{19}$$

Using this sum rule to estimate a_c essentially involves a carrier counting argument. The right side of the sum rule is evaluated starting with a_c near the large radius end of the size distribution. a_c is then moved down through the size distribution until enough carriers have been found to account for the total integrated absorption observed. In order to evaluate Eq. (19) in this way, several hurdles must be gracefully leapt. It is necessary to approximate the absorption integral using a finite frequency range and to obtain estimates for $\eta(\omega)$ and ω_p. The primary free-carrier contribution to the absorption integral comes from the sphere resonance, so that only a small error will result from limiting the range of the integration to those frequencies for which the sphere resonance is significant. Because the sphere resonance is near the CsI reststrahl the data must be extrapolated into the reststrahl region to obtain absorption values over a large enough frequency region.

This extrapolation was performed by fitting a Lorentzian line shape to the low-frequency edge of the sphere resonance and then using the fitted curve as the absorption value for frequencies for which data do not exist. The resulting absorption curve should approximate the absorption that would result by placing the same Bi particles in a "fictitious" nonabsorbing host having a frequency-independent dielectric constant equal to that of CsI above its reststrahl. The fitted extension used for powders 1–5 is shown in Fig. 12 down to 100 cm^{-1}, but the extension

is of course continued to zero frequency. The most drastic extrapolation necessary was for Bi powder 1, which of all samples had its sphere resonance closest to the reststrahl region.

The real part of the index of refraction for the CsI/Bi particle composite was not measured, but a reasonable estimate may be found using the Maxwell-Garnett effective-medium theory[20] and the angular average of the anisotropic dielectric function of Bi. The dielectric constant of CsI above its reststrahl[21] was used as the dielectric constant for the fictitious frequency-independent nonabsorbing host appropriate for use with the extrapolated data. Significant frequency dependence of the composite index is only apparent around the region of the Bi particle sphere resonance, but even there the change is less than 1%. For the evaluation of a_c, the value $n=1.59$ is used.

The plasma frequency of bismuth may be found from the carrier number density and effective masses, but it isn't clear which elements of the anisotropic mass tensors to use or how to average over the anisotropy. Instead, the plasma frequency is estimated using the observed frequency of the sphere resonance. The sphere resonance should behave at least approximately according to the Mie theory[22,23] result for an isotropic plasma, for which the resonance frequency in the absence of damping is given by

$$\omega_R=\frac{\omega_p}{\sqrt{\epsilon_L+2\epsilon_0}} . \tag{20}$$

Using $\epsilon_L=60$ for the contribution of core polarization to the dielectric function of Bi and $\epsilon_0=2.5$, and substituting the observed sphere resonance frequency of approximately 200 cm^{-1}, the plasma frequency is about 1600 cm^{-1}. This is consistent with direct calculations based on n and m^*, which give frequencies ranging from 1100 to 2050 cm^{-1}.

The absorption for five Bi powders showed a sphere resonance, but for one of these, powder 3, a size distribution was not available. The values of the critical radius a_c obtained for those powders that could be analyzed were 130, 90, 140, and 100 nm for powders 1, 2, 4, and 5, respectively. Given the assumptions that went into the analysis, these values are remarkably consistent. The immediate implication is that particles with a diameter larger than approximately 200 nm are responsible for the observed field-dependent absorption which, at least in the largest particles, is successfully described by the semiclassical model.

VI. CONCLUSIONS

While the single-component plasmas found in semiconductor structures show similar field-dependent absorption behavior for both semiclassical[3] and quantum confinement,[4–10] the multicomponent carrier plasma in small bismuth particles shows a dramatic qualitative change in behavior with decreasing size. As particle sizes are reduced from 0.5 μm to 150 Å, magneto-optical absorption of small bismuth particles changes radically from an abundance of field-dependent resonances to strong, field-independent absorption. Qualitative arguments relate the change with the effects of confinement. More quantitative information can be obtained despite broad particle size distributions through the use of a size-specific sum-rule analysis. This approach sets a rough lower limit of 200 nm on the diameter of particles responsible for the observed field-dependent absorption.

It would be interesting to repeat this experiment with substantially improved samples. A tantalizing possibility would be to use some of the advanced fabrication techniques developed for semiconductors to grow quantum dots of bismuth. It has already been shown that high-quality thin films of Bi can be grown by molecular-beam epitaxy on barium fluoride (BaF_2) substrates.[24] BaF_2 does have some optical structure in the FIR frequency region, but successful FIR studies of such films have been done.[25] Nanolithography techniques could then be used on these films to create arrays of Bi dots. This would produce a sample without significant size or orientation distributions. Unlike semiconductor quantum dots, however, the Bi quantum dot system should show a striking qualitative change in behavior between the semiclassical and quantum limits.

ACKNOWLEDGMENT

This work was supported by the Office of Naval Research Contract No. N00014-85-K-0808.

*Present address: Solid State Electronics Directorate, Research Division, WL/ELRA Wright Patterson AFB, OH 45433.

[1] *Electrical Transport and Optical Properties of Inhomogeneous Media,* Proceedings of The First Conference on The Electrical Transport and Optical Properties of Inhomogeneous Media, edited by J. C. Garland and D. B. Tanner, AIP Conf. Proc. No. 40 (AIP, New York, 1977).

[2] ETOPIM2: Proceedings of the Second International Conference on Electrical Transport and Optical Properties of Inhomogeneous Media [Physica A **157** (1989)].

[3] S. J. Allen, Jr., H. L. Stormer, and J. C. M. Hwang, Phys. Rev. B **28**, 4875 (1983).

[4] Ch. Sikorski and U. Merkt, Phys. Rev. Lett. **62**, 2164 (1989).

[5] J. Alsmeier, E. Batke, and J. P. Kotthaus, Phys. Rev. B **41**, 1699 (1990).

[6] T. Demel, D. Heitmann, P. Grambow, and K. Ploog, Phys. Rev. Lett. **64**, 788 (1990).

[7] K. Kern, T. Demel, D. Heitmann, P. Grambow, Y. H. Zhang, and K. Ploog, Superlatt. Microstruct. **9**, 11 (1991).

[8] K. Kern, D. Heitmann, P. Grambow, Y. H. Zhang, and K. Ploog, Phys. Rev. Lett. **66**, 1618 (1991).

[9] A. Lorke and J. P. Kotthaus, Superlatt. Microstruct. **9**, 103 (1991).

[10] W. Hansen, T. P. Smith III, K. Y. Lee, J. A. Brum, C. M. Knoedler, J. M. Hong, and D. P. Kern, Phys. Rev. Lett. **62**, 2168 (1989).

[11]R. E. Sherriff and R. P. Devaty, Phys. Rev. B **41**, 1340 (1990).
[12]R. P. Devaty, Phys. Rev. B **38**, 7972 (1988).
[13]R. P. Devaty and R. E. Sherriff, in *Physical Phenomena in Granular Materials,* edited by G. D. Cody, T. H. Geballe, and P. Sheng, MRS Symposia Proceedings No. 195 (Materials Research Society, Pittsburgh, 1990), p. 15.
[14]C. G. Granqvist and R. A. Buhrman, J. Appl. Phys. **47**, 2200 (1976).
[15]E. I. Du Pont de Nemours and Company, Inc., Plastic Products and Resins Department, Fluoropolymers Division, Wilmington, DE 19898.
[16]S. Lee, T. W. Noh, and J. R. Gaines, Phys. Rev. B **32**, 3580 (1985).
[17]H. O. McMahan, J. Opt. Soc. Am. **40**, 376 (1950).
[18]L. Brey, N. F. Johnson, and B. I. Halperin, Phys. Rev. B **40**, 10 647 (1989).
[19]G. L. Carr, R. L. Henry, N. E. Russell, J. C. Garland, and D. B. Tanner, Phys. Rev. B **24**, 777 (1981).
[20]R. Landauer, in *Electrical Transport and Optical Properties of Inhomogeneous Media* (Ref. 1), p. 2.
[21]W. L. Wolfe and G. J. Zissis, *The Infrared Handbook* (Office of Naval Research, Department of the Navy, Arlington, VA, 1978).
[22]G. Mie, Ann. Phys. (Leipzig) **25**, 377 (1908).
[23]H. C. van de Hulst, *Light Scattering by Small Particles* (Dover, New York, 1981).
[24]D. L. Partin, J. Heremans, D. T. Morelli, C. M. Thrush, C. H. Olk, and T. A. Perry, Phys. Rev. B **38**, 3818 (1988).
[25]S. Takaoka and Kazuo Murase, J. Phys. Soc. Jpn. **54**, 2250 (1985).